Article ID: 1007-7294(2024)12-1908-17

Numerical Simulation of Multiple Collisions Between Ice Ridge and Polar Ship

JIA Bin[1], *JU Lei*[1], *SHI Li*[2], *WANG Qing*[1], *PANG Fu-zhen*[1]
(1. College of Shipbuilding Engineering, Harbin Engineering University, Harbin 150001, China;
2. American Bureau of Shipping (China) Co., Ltd., Shanghai 200001, China)

Abstract: Ships navigating in ice-covered regions will inevitably collide with ice ridges. Compared to other ice bodies, ice ridges exhibit more complicated mechanical behaviors due to the scale and structure characteristics. In this paper, nonlinear finite element method is used to investigate the interaction between a polar ship and an ice ridge. The ice ridge is modelled as elastic-plastic material based on Drucker-Prager yield function, with the consideration of the influence of cohesion, friction angle and material hardening. The material model is developed in LS-DYNA and solved using semi-implicit mapping algorithm.The stress distribution of ice ridge and ship, and the ice load history are evaluated through the simulation of multiple collisions. In addition, parametric analysis is performed to investigate the influence of ridge thickness and impact velocity on the ice load and energy absorption.

Key words: ice ridge; ship; nonlinear FEM; ice load; interaction; strength
CLC number: P731.15 P751 **Document code:** A **doi:** 10.3969/j.issn.1007-7294.2024.12.008

0 Introduction

Ice ridge is formed by the freeze of stacked ice piles. It is common in cold regions and its larger size up to a few dozen meters would cause a higher ice load on nearby ships in operations, leading to unexpected structural damage. First-year ice ridges in Gulf of Bothnia and Northumberland Strait even determine the design load levels for marine structures[1]. Due to complex mechanical properties and potential destructiveness of ice ridges, reasonable modelling of the interaction between ice ridge and ship is of vital significance.

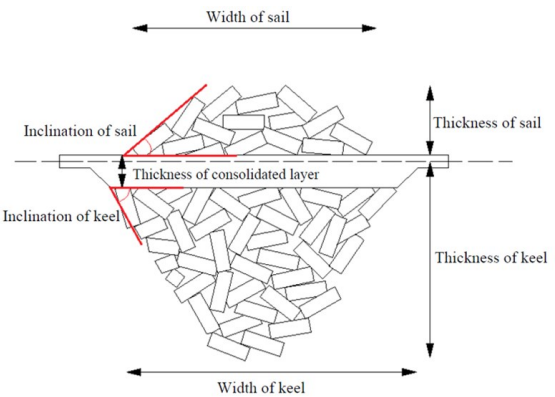

Fig.1 Typical structure of ice ridge

As shown in Fig.1, a typical ice ridge mainly consists of three parts: (1) sail, which is the small part above the waterline and consists of stacked

Received date: 2024-04-19
Foundation item: Supported by the National Natural Science Foundation of China (52192690; 52192695)
Biography: JIA Bin(1994-), male, Ph.D. candidate; JU Lei(1986-), male, Ph.D., associate professor,
E-mail: julei@hrbeu.edu.cn.

ice blocks, which has pores that are filled with air; (2) keel, which is the pile of ice blocks that are loosely or partly consolidated below the waterline, and has pores filled with water and even air pockets; (3) consolidated layer, which is the refrozen layer around the waterline that connects the sail and keel[2-4]. Ice ridges vary in size, Timco and Burden[5] proposed equations to describe the geometric characteristics of the ridges based on the analysis of salient features of 112 first-year and 64 multi-year sea ice ridges. Furthermore, the mechanical properties of ice ridge were prevailingly investigated based on in-situ full-scale and model-scale tests, through which the shear strength of keel, the flexural and compressive strength of the consolidated layer, etc. have been evaluated[1, 6-10].

The previous studies about the interaction between ice ridges and marine structures were carried out based on theoretical analysis[11-15] and experimental studies[16-21]. Due to higher computational efficiency and remarkable applicability, numerical methods have been widely used in simulations that are related to ice bodies. Since most part of an ice ridge is made of individual ice blocks, Discrete Element Method (DEM) is widely considered as an effective numerical method to describe the deformation and failure of ice ridges. Sawamura[22] simulated the accumulation of ice piles and modelled the 2D/3D interaction between ice ridge and ship. Gong et al[2-3] studied the resistance of ship in an unconsolidated ridge, which demonstrated the major effect of ridge width on the resistance. Molyneux et al[23] analyzed the load during the interaction between the first-year ice ridges and a vertical cylinder using discrete element code (DECICE), and pointed out the importance of the involvement of cohesion among ice blocks in numerical simulation. Besides, Polojärvi[24] established a combined finite-discrete element framework to imitate the freeze bonds, which takes both the deformation of ice blocks and contact among the ice blocks into account.

Due to general continuity inside ice ridges and the specific material properties of ice ridges, finite element method (FEM) has also been applied to the related numerical models. FEM provides various material models (elastic-plastic models, visco-plastic models, etc.), and is convenient for secondary development to precisely model ice ridges. Heinonen[1] presented a constitutive ice ridge-model based on cohesive softening and multiple failure surfaces, and simulated the punch shear test in ABAQUS; Serré[25] proposed a softening model, in which the cohesion decreases linearly so that the freeze bonds failure in the ice blocks could be represented. In addition, FEM is effective for the structural evaluation of ship hulls under ice load. Zhao et al[26] conducted structure analysis of a heavy icebreaker during ramming of first-year ridges, in which the local ice-induced pressure on the hull and subsequent structural responses were discussed.

Multiple collisions between ice ridge and ships are not just simple repeated impacts, while former collision would weaken the strength of ice ridge before the next collision occurs. According to Timco′s in-situ punch tests: when load exerted on the ridge reaches its first peak, a large number of freeze bonds among inner ice blocks fail, which leads to the breakage of ice blocks and overall strength reduction of ridge; when the second collision occurs, free ice blocks break into smaller pieces and fill the inner gaps. The ice ridge is compacted under compression, which is related to the second peak in the load curve. Due to failure of freeze bonds among ice blocks and change of cohe-

sion and friction angle after the first collision, the second peak value is obviously lower than the first one[27]. Variations of material properties of an ice ridge during multiple collisions are mainly featured as follows: (1) cohesion decrease caused by the failure of freeze bonds; (2) variation of friction angle due to the free motion and compaction of ice blocks; (3) material hardening caused by gaps filling and relative motion of ice blocks.

In this paper, multiple collisions between ship and ice ridge are numerically modelled using LS-DYNA software. Ice ridge is modelled as elastic-plastic material using secondary development program, in which the Drucker-Prager yield function is induced and further modified according to the characteristic variations during the multiple collisions. Based on the simulation of multiple ridge-ship collisions, the stress/strain distribution and energy absorption of ice ridge, motion of the ship and ice load history are obtained and analyzed.

1 Material model of ice ridge

1.1 Constitutive relation

Ice ridge is formed by freezing discrete stacked ice blocks, with its internal space filled with air, water and impurities. It exhibits more complexity than other ice bodies. Ettema and Urroz, Timco and Cornett[28-29] carried out a series of shear tests and proposed that the mechanical behaviors of ice ridge could be modelled as elastic-plastic material. Then Heinonen, Serré and Wong et al[1, 25, 30] validated this material model and made improvements based on different yield criteria. In this paper, isotropic elastic-plastic model is used to describe the deformation of ice ridge. The total strain $\boldsymbol{\varepsilon}_{ij}$ could be decomposed into elastic strain $\boldsymbol{\varepsilon}_{ij}^{\mathrm{e}}$ and plastic strain $\boldsymbol{\varepsilon}_{ij}^{\mathrm{p}}$

$$\boldsymbol{\varepsilon}_{ij} = \boldsymbol{\varepsilon}_{ij}^{\mathrm{e}} + \boldsymbol{\varepsilon}_{ij}^{\mathrm{p}} \tag{1}$$

When ice ridge is elastic, the constitutive relation satisfies

$$\boldsymbol{\sigma}_{ij} = \boldsymbol{C}_{ijkl}\boldsymbol{\varepsilon}_{kl}^{\mathrm{e}} \tag{2}$$

where, $\boldsymbol{\sigma}_{ij}$ is the stress tensor and $\boldsymbol{C}_{ijkl}$ is the elastic coefficient tensor. In the case of the associated flow rule, the plastic strain rate is

$$\dot{\boldsymbol{\varepsilon}}_{ij}^{\mathrm{p}} = \lambda \frac{\partial f}{\partial \boldsymbol{\sigma}_{ij}} \tag{3}$$

where, f is the yield function, and λ is the plastic consistency parameter. The volumetric plastic strain rate and equivalent deviatoric plastic strain rate are relatively expressed as follows:

$$\dot{\varepsilon}_{\mathrm{vol}}^{\mathrm{p}} = -\lambda \frac{\partial f}{\partial p} \tag{4}$$

$$\dot{\varepsilon}_{\mathrm{dev}}^{\mathrm{p}} = \lambda \frac{\partial f}{\partial q} \tag{5}$$

where q is the second stress invariant and p is the hydrostatic pressure.

1.2 Yield criterion and modification

Ettema and Urroz, Timco and Cornett, and ISO[28-29, 31] recommended that Mohr-Coulomb (M-C) yield criterion be applicable for the constitutive modelling of ice ridge in numerical simulation. Besides, Drucker-Prager (D-P) yield criterion further induces smooth approximation, and the yield

function is

$$q - d - p\tan\beta = 0 \tag{6}$$

where d is the cohesion and β is the friction angle. Though shear failure has been involved, D-P yield criterion is not sufficient to precisely describe the plastic behaviors of ice ridge. At latter stage of interaction, the cohesion fails and the macroscopic gaps inside the ice ridge provide space for the relative motion of free ice blocks and filling of broken ones, which directly leads to the volumetric change. Ice blocks are compacted under compression, causing a distinct increase in strength of ridge. Thus, a new yield surface is defined for the latter stage of interaction when compression predominates, and the strength increase of ice ridge directly related to the volume is described using plastic hardening. The yield surface is shown in Fig.2.

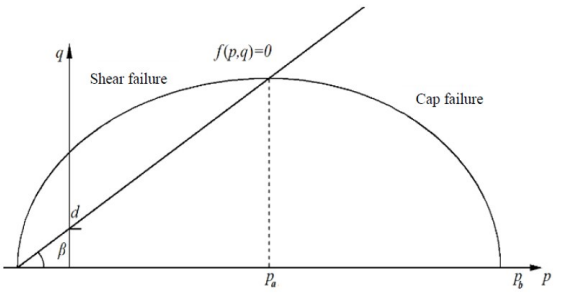

Fig.2 Revised yield surface

If $p \leqslant P_a$, the shear yield surface

$$f_s = \sqrt{\left[\left(p - P_a\right)\tan\beta\right]^2 + q^2} - \left(d + P_a\tan\beta\right) \tag{7}$$

and if $p > P_a$, the compression yield surface

$$f_c = \sqrt{\left(p - P_a\right)^2 + \left(Rq\right)^2} - R\left(d + P_a\tan\beta\right) \tag{8}$$

where R is a parameter that defines the shape of shear yield surface, and P_a is a hardening variable that determines the type of yield surface, which could be obtained from

$$P_a = \frac{P_b - Rd}{1 + R\tan\beta} \tag{9}$$

where

$$P_b = P_0 e^{-\frac{\varepsilon_{vol}^p - \varepsilon_{vol}^p|_0}{\kappa_0}} \tag{10}$$

where P_0 is the hydrostatic pressure, $\varepsilon_{vol}^p|_0$ is the plastic volumetric strain at the reference state, and κ_0 is a softening parameter, the value of which is typically set to 0.03 according to Heinonen's in-situ punch tests[1, 32].

The cohesion strength of ice ridge

$$d = d_0 e^{-\frac{\varepsilon_{dev}^p}{\varepsilon_\infty}} \tag{11}$$

where d_0 is the initial cohesion strength and ε_∞ is the cohesion decrease rate.

In addition, Cam model is introduced into D-P yield criterion so that the strength change of ice ridge under the effect of shear and the variation of friction angle in plastic deformation could be involved[33]. Cam model is defined as

$$\frac{\varepsilon_{dev}^p - \varepsilon_{dev}^p|_0}{\varepsilon_{vol}^p - \varepsilon_{vol}^p|_0} = \frac{2\sin\varphi}{\left(M/\sqrt{3}\right)^2 - \left(\sin\varphi\right)^2} \tag{12}$$

where, $\varepsilon_{\mathrm{dev}}^{\mathrm{p}}|_0$ is the plastic deviatoric strain at the reference state, φ is the friction angle in the M-C yield function, and M is the critical constant that could be evaluated based on the fitting results of triaxial tests[34]. As shown in Fig. 3, M could be approximately expressed as a linear function of initial friction angle φ_0.

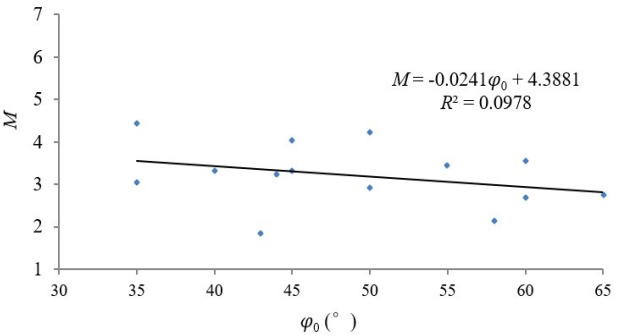

Fig.3 Fitted results of critical constant M

It is noted that $\tan\beta = \sqrt{3}\sin\varphi$ due to shear action, so that

$$\tan\beta = \frac{1}{2}\sqrt{3\cdot\left(\frac{\varepsilon_{\mathrm{dev}}^{\mathrm{p}} - \varepsilon_{\mathrm{dev}}^{\mathrm{p}}|_0}{\varepsilon_{\mathrm{vol}}^{\mathrm{p}} - \varepsilon_{\mathrm{vol}}^{\mathrm{p}}|_0}\right)^2 + 4M^2} - \frac{\sqrt{3}}{2}\frac{\varepsilon_{\mathrm{dev}}^{\mathrm{p}} - \varepsilon_{\mathrm{dev}}^{\mathrm{p}}|_0}{\varepsilon_{\mathrm{vol}}^{\mathrm{p}} - \varepsilon_{\mathrm{vol}}^{\mathrm{p}}|_0} \tag{13}$$

1.3 Failure criterion

During plastic deformation, the stress of ice ridge will flow on the yield surface until the failure occurs. Nevertheless, there is no widely accepted failure criterion yet. Considering that ice ridge is compacted and broken ice blocks flow out from gaps between ice ridge and ship like viscous fluid in the latter stage of interaction, it is reasonable to apply the failure criterion of icebergs for the ice ridge. Based on the empirical failure criterion of icebergs, the elements of ice ridge[35-36] are assumed to fail if

$$\varepsilon_{\mathrm{eq}}^{\mathrm{p}} > \varepsilon_{\mathrm{f}} \tag{14}$$

or

$$p < p_{\mathrm{c}} \tag{15}$$

where

$$\varepsilon_{\mathrm{f}} = \varepsilon_0 + \left(\frac{p}{10^8} - 0.5\right)^2 \tag{16}$$

where, ε_{f} is the failure strain, ε_0 is the initial failure strain, and p_{c} is the cut-off pressure.

2 Numerical implementation and validation

2.1 Numerical model

Semi-implicit backward Euler algorithm features higher stability, and avoids the solution of plastic flow direction and plastic modulus gradient as well. In this paper, semi-implicit mapping algorithm is adopted, and the material model of ice ridge is encoded in the secondary-developed dynamic link library LSDYNA.LIB (dyn21). The plastic deformation is calculated based on incremental theory so that stress could be obtained from constitutive relation according to incremental strain in each time step. The calculation procedures in each time step are shown in Fig.4. The constant d, P_b and β are calculated based on Formulas (11), (10) and (13).

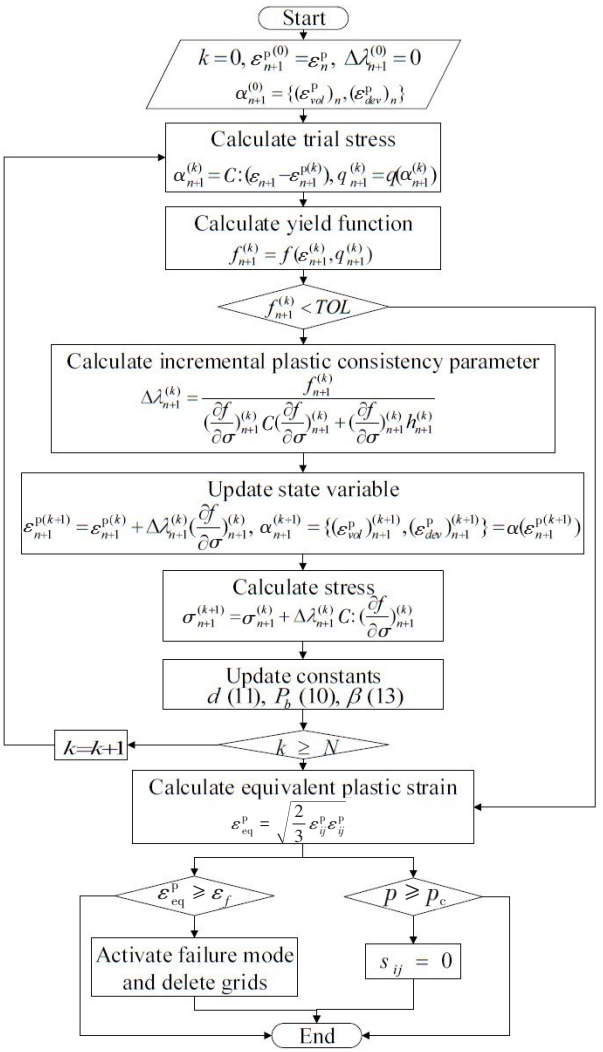

Fig.4 Flow chart of the calculation of constitutive model

Elastic strain will firstly appear in the ice ridge after the first ridge–ship collision occurs. Then with the increase of impact force, ice ridge undergoes plastic deformation and starts to break when it reaches the critical failure state. The kinematic velocity of ship decreases due to resistance induced by the ice ridge. When the velocity decreases to zero, there is no actual contact between the ice ridge and ship so that it enters unloading phase, where elastic strain vanishes while plastic strain remains the same. Before the numerical calculation for the next collision, the cohesion, friction angle, yield surface of shear failure or compression failure around the contact area are no longer the same, which should be determined by the plastic strain at current time step. Therefore, the variations of cohesion, friction angle and material hardening are described using state variables and equivalent plastic strain, and parameters like stress and strain could be precisely transmitted to numerical model for the next collision.

Explicit central difference algorithm is used to solve the governing equation. The differential equation of motion in time step n is

$$\boldsymbol{M}\cdot\ddot{\boldsymbol{x}}(t_n)+\boldsymbol{C}\cdot\dot{\boldsymbol{x}}(t_n)+\boldsymbol{K}\cdot\boldsymbol{x}(t_n)=\boldsymbol{F}_n^{ex} \tag{17}$$

where $\boldsymbol{M}$、$\boldsymbol{C}$ and $\boldsymbol{K}$ represent the mass, damp and stiffness matrix of structure, respectively. $\boldsymbol{F}_n^{\text{ex}}$ is the matrix of external force and $\boldsymbol{x}$ is the nodal displacement. It can also be written as

$$\ddot{\boldsymbol{x}}\left(t_n\right)=\boldsymbol{M}^{-1}\left(\boldsymbol{F}_n^{\text{ex}}-\boldsymbol{F}_n^{\text{int}}\right)=\boldsymbol{M}^{-1}\boldsymbol{F}_n^{\text{residual}} \tag{18}$$

where, $\boldsymbol{F}_n^{\text{int}}=\boldsymbol{C}\cdot\dot{\boldsymbol{x}}\left(t_n\right)+\boldsymbol{K}\cdot\boldsymbol{x}\left(t_n\right)$ is the matrix of internal force and $\boldsymbol{F}_n^{\text{residual}}$ is the matrix of residual load. The velocity vector at time $t_{n+1/2}$ and coordinate vector of node at time t_{n+1} could be calculated based on the acceleration of node as

$$\dot{\boldsymbol{x}}\left(t_{n+1/2}\right)=\dot{\boldsymbol{x}}\left(t_{n-1/2}\right)+\ddot{\boldsymbol{x}}\left(t_n\right)\left(\Delta t_{n+1/2}+\Delta t_{n-1/2}\right)/2 \tag{19}$$

$$\boldsymbol{x}\left(t_{n+1}\right)=\boldsymbol{x}\left(t_n\right)+\dot{\boldsymbol{x}}\left(t_{n+1/2}\right)\Delta t_{(n+1)/2} \tag{20}$$

The calculation procedures are shown in Fig.5.

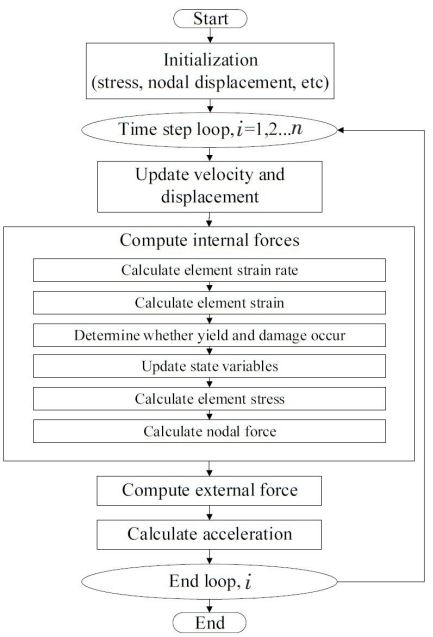

Fig.5 Flow chart of the LS-DYNA solver

In order to ensure the numerical stability and avoid contact penetration, the time step in explicit algorithm should satisfy

$$\Delta t\leqslant 2/w_{\max} \tag{21}$$

where $w_{\max}$ is the maximum natural frequency of the structure. For hexahedral element,

$$\Delta t_{\min}=V/\left[A_{\max}\sqrt{\frac{E(1-\mu)}{(1+\mu)(1-\mu)\rho}}\right] \tag{22}$$

where, $A_{\max}$ represents the maximum element area, E is the elastic modulus, μ is the Poisson ratio and ρ is the density of material.

2.2 Validation

The material model is validated through the simulation of the ridge-cone interaction, and the numerical results are compared with experimental data from model tests performed at HSVA on behalf of Aker Solutions. The geometric properties of cone and ice ridge are the same as that in Ref. [21]. The ice ridge is modelled using solid elements and material properties are shown in Tab.1.

Since both the rigid cone and ice ridge are relatively large in size, the influence of water is neglected in this section. Both ends of ice ridge are of fixed, non-reflective boundary. The type of contact between ice ridge and ship is set as *CONTACT-ERODING-SURFACE-TO-SURFACE, and the static and dynamic friction coefficients are 0.11 and 0.05, respectively. Due to huge strength difference between the ice ridge and ship, softened contact constraint algorithm and "Surface to Surface" search method are used to reduce the numerical error. The impact velocity is 0.2 m/s.

Tab.1 Material parameters of ice ridge

Parameter	Unit	Value	Parameter	Unit	Value
Density	kg/m^3	900	κ	–	0.03
Poisson ratio	–	0.3	R	–	2
Elastic modulus	MPa	5.7	M	–	3.54
Initial failure strain	–	0.01	P_C	MPa	−4
Initial friction angle	(°)	35	ε_f	–	0.35
Cohesion	kPa	7			

Fig.6(a) presents the calculated history of horizontal ice load during the cone-ridge collision, and both variation tendency and the peak load agree well with the experimental results. It should be noted that the numerical error mainly comes from the structural distinctions, as the ridge in model test exhibits more randomness while that in numerical model are more ideal and conceptual.

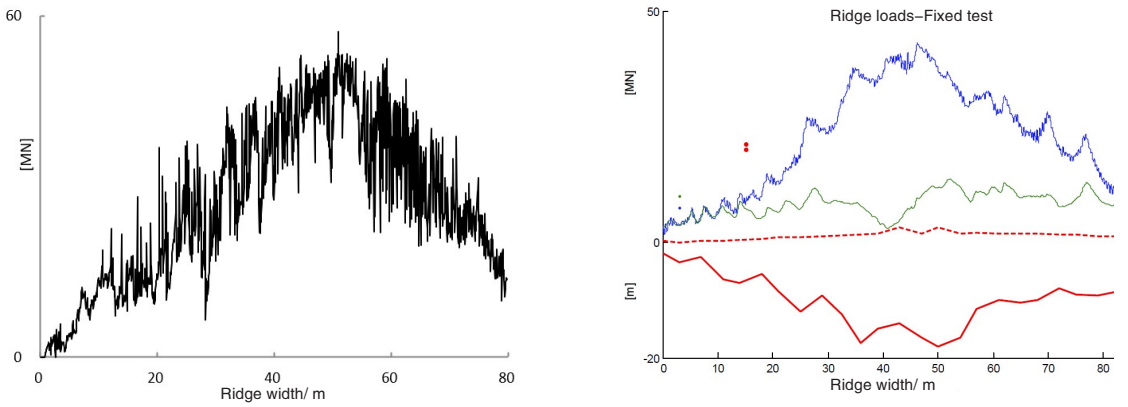

(a) Numerical results　　(b) Test results from Aker[21]

Fig.6 History of horizontal ice load

3 Numerical simulation

3.1 Numerical model

The ship model used in this paper is based on Xuelong icebreaker, with a displacement of 18 102.4 tons. Since the icebreaking performance of the ship and the damage of ice ridge are research priorities, only the hull shell is modelled using shell elements with certain thickness. The shell thickness is determined according to the assumption that the weight of shell is equal to the displacement. In addition, the motion of water will cause additional water mass during the ship-ridge interaction. Additional water mass is related to the hull shape, motion characteristics and the ship-ridge interaction, which is about 0.02 to 0.07 times the hull mass[37]. In this paper, the additional water mass is set to 0.05 times the hull mass, which is achieved by increasing the shell thickness by

0.012 m. Furthermore, the grids around the bow are refined so that the contact in this area could be captured precisely. The hull material is modelled as elastic model, and the parameters are listed in Tab.2.

Tab.2 Material parameters of ship hull

Parameter	Unit	Value
Density	kg/m^3	7850
Elastic modulus	GPa	200
Poisson ratio	–	0.3

The contact type is the same as that in Section 2.2, except that the dynamic friction coefficient is 0.11 according to Ref.[38]. Besides, in order to model the semi-infinite ridge and weaken the boundary effects, the width of ice ridge is taken much larger than ship breadth. The side that collides with the ship is set as free boundary, while the other sides are fixed and non-reflective boundary. The material parameters of ice ridge are the same as those listed in Tab.1. The geometric characteristics and parameters of ice ridge are shown in Fig.7 and Tab.3.

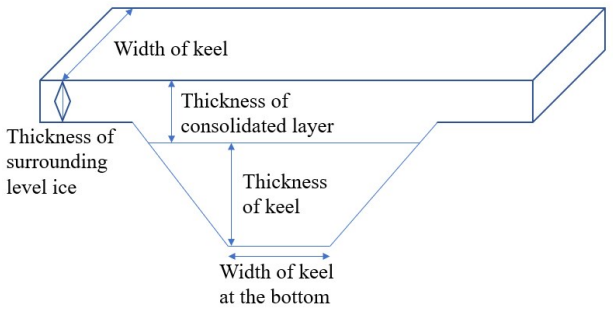

Fig.7 Geometric characteristics of ice ridge

Tab.3 Geometric parameters of ice ridge

Parameter	Unit	Value
Thickness of surrounding level ice	m	0.83
Thickness of consolidated layer	m	3.1
Keel thickness	m	5.73
Keel width	m	240
Keel bottom width	m	36
Keel angle	°	29.6
Macro-porosity of keel	%	20

The ship is kept in upright condition, and moves towards the ice ridge with an initial velocity of 2 m/s. If the ship starts to exit from the inside of ice ridge, the same initial velocity is applied on the ship again to drive the next collision. Furthermore, the plastic strain and residual grid of ice ridge will remain unchanged before the next collision occurs. The steps above are repeated until the ship completely penetrates the ice ridge.

3.2 Numerical results

Fig.8 illustrates the strain distribution of ice ridge after the second collision, which indicates that the elastic strain has mostly disappeared and only exists in a small part of the outer ice ridge that is still in contact with the hull. However, the plastic strain remains in the ice ridge, which leads to lower structural strength of ice ridge compared to that before the previous collision. Therefore, the part of ice ridge with existing plastic strain is more likely to fail in the subsequent collisions.

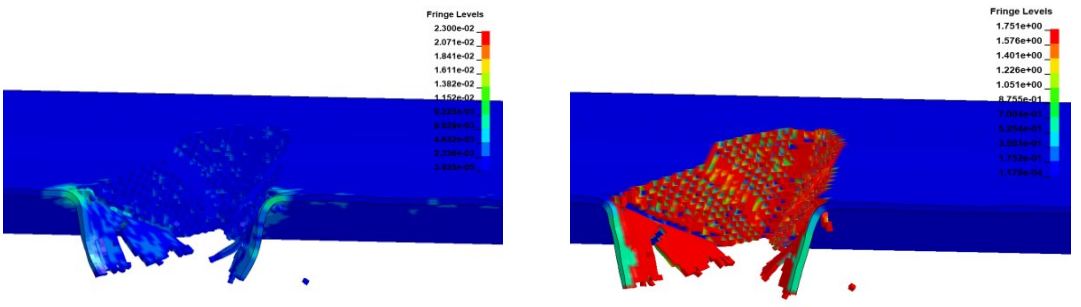

(a) Elastic strain (b) Plastic strain

Fig.8 Strain distribution of ice ridge after the second collision

The damage and stress distribution of ice ridge after the first three collisions are shown in Fig.9. The higher stress is mainly concentrated on the surface that is in contact with the ice ridge. Besides, the stress of ship hull in Fig.10 indicates that the areas under significant compression are mainly the load-bearing parts, like stem post and outer shell around the bow, which should be strengthened in structural design.

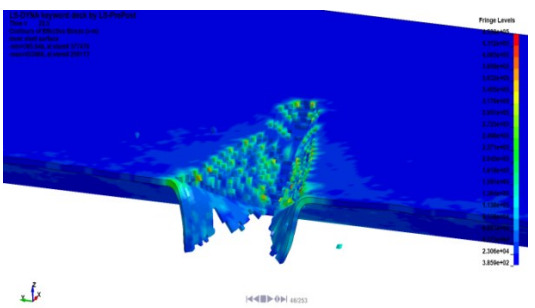

(a) t = 22.5 s [3.859E+02~4.539E+05]

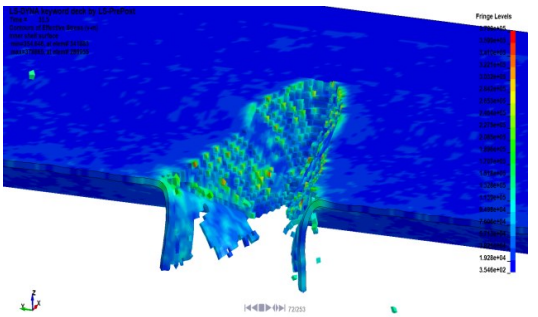

(b) t = 35.0 s [3.545E+02~3.789E+05]

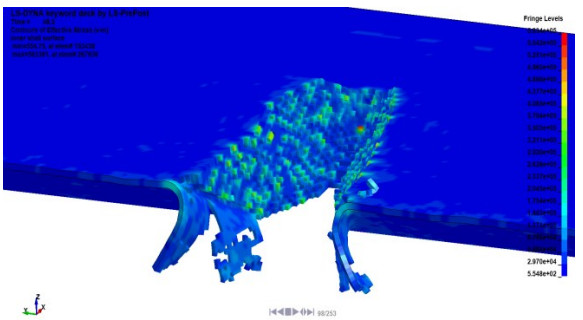

(c) t = 48.5 s [5.548E+02~5.834E+05]

Fig.9 von Mises stress of ice ridge after multiple collisions

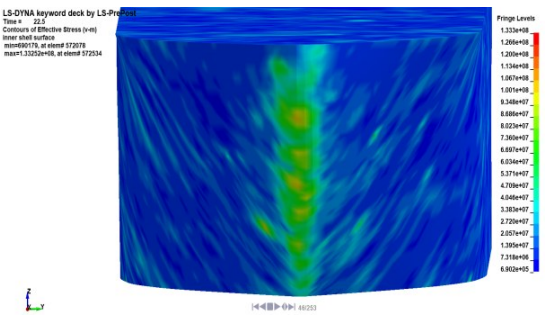

(a) t = 22.5 s [6.902E+05~1.333E+08]

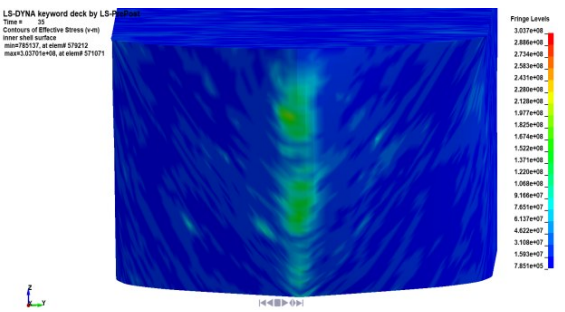

(b) t = 35.0 s [7.851E+05~3.037E+08]

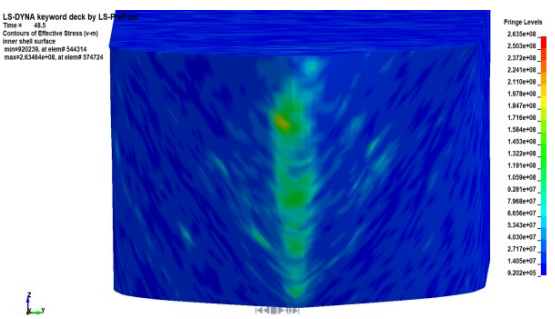

(c) t = 48.5 s [9.202E+05~2.635E+08]

Fig.10 von Mises stress of ship hull after multiple collisions

During each collision, the ice load will increase as ship enters the inside of ice ridge. And the elements of ice ridge will be deleted if they reach the critical failure state, causing the formation of gaps between ridge and ship and the unloading of contact force. Since the bow has not entered the ice ridge sufficiently and the ridge thickness around the contact zone is relatively lower during the first collision, the ice load in this period would be lower than that in the subsequent ones. Details about ice load will be discussed in Chapter 4. The velocity history of ship in Fig.11 illustrates that the velocity decreases more slowly in the first collision than those in the other ones, which is related to the lower ice load in this period. Thus, this lower ice load also causes larger displacement, as shown in Fig.12. When the ship hull enters the inside of ice ridge in subsequent collisions, there is no significant difference in the ridge thickness anymore. Therefore, similar variation characteristics are concluded for velocity/displacement during the second and third collisions.

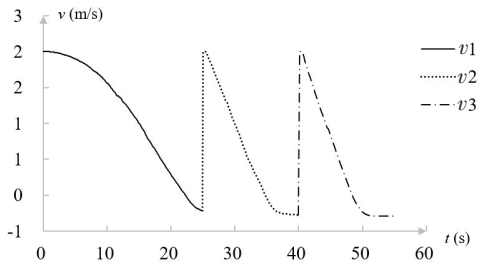

Fig.11 Velocity history of ship during multiple collisions (*vn* represents the velocity during the *n*th collision)

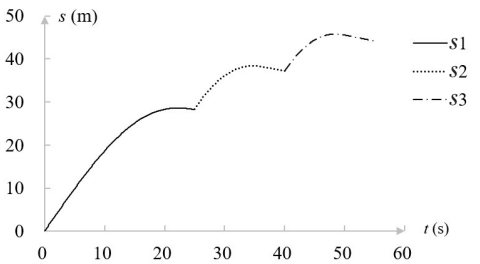

Fig.12 Displacement history of ship during multiple collisions (*sn* represents the displacement during the *n*th collision)

4 Discussion

The influence of ridge thickness and impact velocity on the ridge–ship collision is investigated in this chapter. The ice ridge thickness here is defined as

$$T = T_k + T_c - T_l \tag{23}$$

where T_k is the keel thickness, T_c is the consolidated layer thickness, and T_l is the level ice thickness. If the keel thickness is too high, excessively high upward force caused by the crushed ice below the ship bottom would lead to trim by the stern, and the ship will lose its ability to move forwards or backwards and strand in the ice ridge. The designed draft for the ship in this paper is 8 m, and the maximum ridge thickness in this chapter is set as twice of it. The initial velocity and ridge thickness in different scenarios are listed in Tab.4.

Tab.4 Initial velocity and ridge thickness in different scenarios

Scenario	1	2	3	4	5
Initial velocity /(m·s^{-1})	2	3	4	3	3
Ridge thickness /m	8	8	8	12	16

The numerical results show that the number of impacts needed for the complete penetration are 6, 3, 2, 3 and 4 respectively for the five scenarios, which is apparently negatively correlated with

the impact velocity and not sensitive to the ridge thickness. Fig.13 shows the ship displacement during each impact in five scenarios. As shown in Fig.14, the ice ridge is almost completely penetrated after the third collision in Scenario 5, and the volume of the remaining ice body is less massive, which means that the ridge will be fully penetrated within a short period of time in the fourth collision. The ship displacement after the last impact will be much larger than that in other scenarios, and there is no actual ship–ridge interaction for a long time. Therefore, the ice load and energy absorption are discussed only when the ship displacement is less than 70 m.

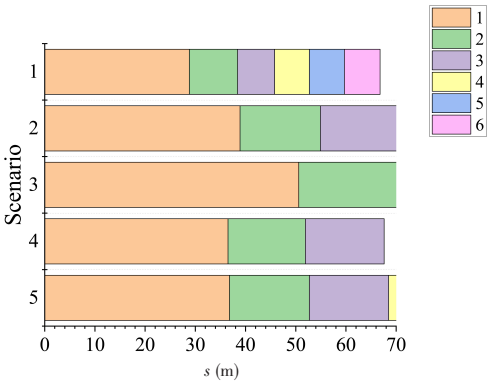

Fig.13　Ship displacement during each impact in different scenarios

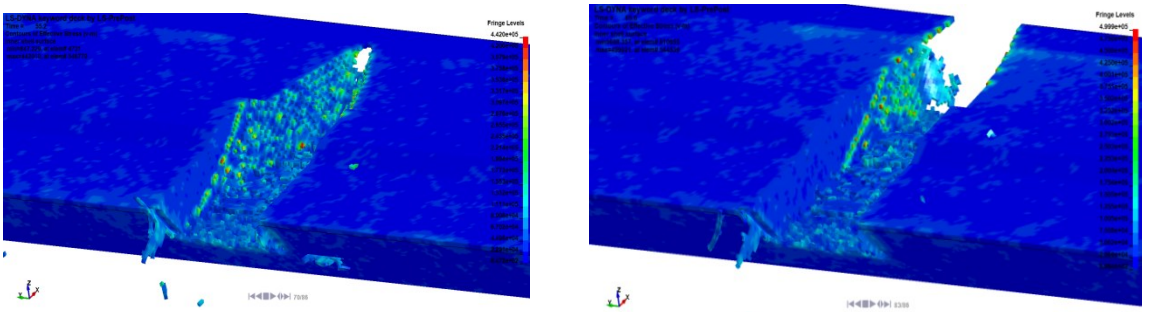

(a) After the third impact [8.472E+02~4.420E+05]　(b) After the fourth impact [6.984E+02~4.999E+05]

Fig.14　von Mises stress of ice ridge in Scenario 5

4.1 Ice load

Fig.15 presents the history of horizontal ice load (F_x) during multiple collisions in five scenarios. During each collision, the ice load increases first and then decreases. The peak horizontal ice load during the first collision exhibits a positive correlation with both impact velocity and ridge thickness. From the perspective of the entire icebreaking process, as the ship enters the ice ridge, the ice load gradually increases with the increase of the thickness of the ice body. When the ship reaches the middle part of the ridge, the ridge thickness maintains at a high level, and the ice load level increases with a lower growth rate. Fig.15 also indicates that the peak ice load during a collision is generally higher than that in the previous collision, and the extreme ice load throughout the whole process usually occurs during the last two collisions. However, when the ship speed is 2 m/s, more impacts are required due to the limited ice-breaking range and lower initial kinematic energy in a single impact. Thus, the lower structural rigidity of residual ridge will directly lead to a slightly lower peak ice load in the last collision. There are no significant differences between the peak ice loads in Scenarios 4 and 5, which indicates that the resistance induced by ice ridge is less likely to be affected if ridge thickness is larger than the designed draft of ship.

Fig.16 demonstrates the fluctuation of F_y around zero during multiple collisions in five scenarios. Considering that the ship is symmetrical about the y–axis, an approximately neutral force condi-

tion in y–direction is reasonable. Higher ice load occurs when the hull is in sufficient contact with the thickest part of the ridge in the later stage, and the magnitude of instant ice load is within 5×10^6 N. Comparative analysis indicates that F_y generally shows positive correlation with both impact velocity and ridge thickness.

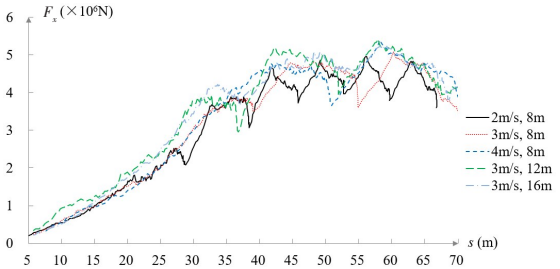

Fig.15 F_x–displacement curves in different scenarios

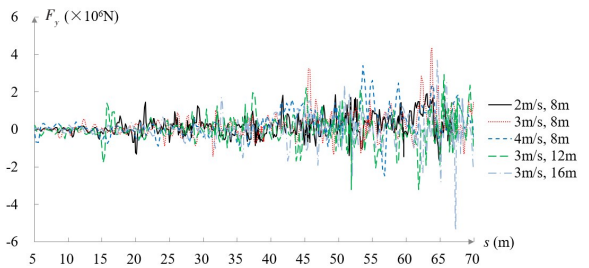

Fig.16 F_y–displacement curves in different scenarios

As shown in Fig.17, the vertical ice load shares many similar characteristics with the horizontal one from the perspective of the entire icebreaking process. Nevertheless, due to the existence of inclined plane on the bow, the magnitude of vertical ice load is obviously larger than that of horizontal load. Ship that rushes to ice ridge with an impact velocity of 4 m/s is subject to higher ice load, while vertical ice load is approximately the same when impact velocity is 2 m/s or 3 m/s. In addition, the vertical ice load increases remarkably with the ridge thickness, while this increase is not evident when ridge thickness is larger than 12 m. This insensitivity is due to the neglect of the pile–on effect caused by the crushed ice at the ship bottom.

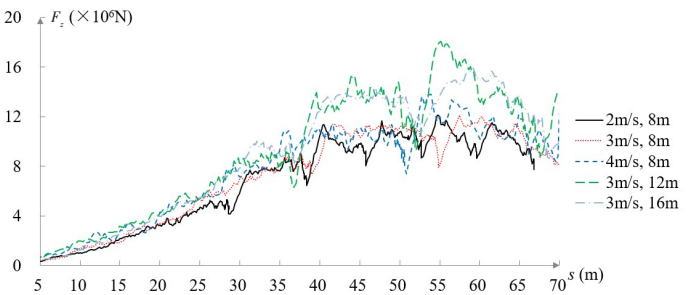

Fig.17 F_z–displacement curves in different scenarios

The statistical results of ice load are listed in Tab.5. The ridge thickness generally has positive correlation with the statistical variables concerning average ice load and peak ice load. The increase of ice load is significant when the ridge thickness increases from 8 m to 12 m, while the difference is less obvious when ridge thickness is 12 m or 16 m. If the designed draft of ship is equal

Tab.5 Statistical results of ice load

	Unit	Scenarios				
		1	2	3	4	5
Average ice load during first collision ($F_x^{(1)}$)	$\times10^6$ N	1.55	2.54	3.23	2.56	2.64
Maximum of average ice load during single collision ($F_{x\_average\_max}$)	$\times10^6$ N	4.23	4.28	4.34	4.62	4.65
Maximum increase of average ice load between adjacent collisions ($F_{x\_incre\_max}$)	%	129	68.5	34.4	80.5	76.2
Maximum F_x($F_{x\,max}$)	$\times10^6$ N	4.85	5.12	5.48	5.53	5.45
Maximum F_y($F_{y\,max}$)	$\times10^6$ N	1.91	4.42	3.49	3.25	5.19
Maximum F_z($F_{z\,max}$)	$\times10^6$ N	12.56	12.48	13.96	18.12	15.23

to the ridge thickness, the ship bottom is hardly affected by the ice body during the impact. When the draft is less than the ridge thickness, there will be residual ice body at the ship bottom when ship penetrates the ice ridge. The high ridge thickness will cause the structural stiffness of the ridge to increase, thereby causing an increase in ice load. When the ridge thickness increases from 1.5 times to 2.0 times the draft, since the interaction area is still mainly concentrated in the upper part of the ice ridge, further increase in the vertical stiffness of the ice ridge structure will not significantly increase the ice load.

It seems that the average horizontal ice load during the first collision is obviously sensitive to the impact velocity, while the influence of ridge thickness could be neglected. On the other hand, numerical results show that the effect of impact velocity and ridge thickness on the maximum of average ice load during single collision is limited. The analysis of maximum increase of average ice load between adjacent collisions indicates that higher impact velocity will lead to a relatively large initial ice load, but subsequent increments will be smaller. Therefore, it is reasonable to conclude that the ship should collide with the ridge with a lower velocity at first and gradually increase the impact velocity in the subsequent collisions, so that the lower ice load and higher ice-breaking efficiency could be ensured.

4.2 Energy absorption

The energy absorption of ice ridge in five different scenarios is shown in Fig.18. Comparative analysis shows that the energy absorption is higher if impact velocity is lower, which illustrates more severe damage inside the ice ridge during approximately static loading. When the impact speed is high, the ice ridge will undergo significant deformation in the impact area in a short period of time, and then fracture and damage will occur. However, there is no extensive deformation at the far end of the ridge, so that the overall deformation energy is lower. In addition, the energy absorption of ridge has generally positive correlation with ridge thickness. It is also reasonable to conclude that the influence of ridge thickness on the ship-ridge interaction is rather weak if the ridge is 0.5 times thicker than the draft, since there is no significant difference in energy absorption and ice load F_x and F_z when ridge thickness is larger than 12 m.

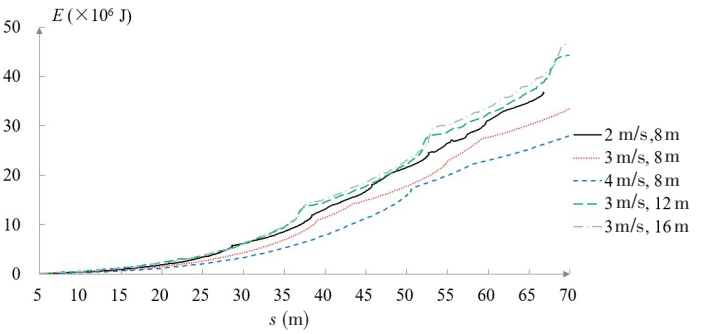

Fig.18 Deformation energy absorbed by ice ridge in different scenarios

5 Conclusions

In this paper, ice ridge was numerically modelled using elastic-plastic model, with the consideration of cohesion, friction angle and material hardening characteristics. The numerical results show that the accumulated damage and failure of ice ridge in multiple collisions could be properly captured through the numerical model proposed. Meanwhile, the stress distribution on ice ridge and

ship hull, motion of ship and ice load are obtained. In addition, parametric analysis based on ridge thickness and impact velocity is carried out. The main conclusions are as follows:

(1) During the entire ship-ridge interaction, the ice load generally shows an increasing trend, with multiple loading-unloading stages. The extreme ice load occurs during the last two collisions, when the ship travels to the position where the thickness of ice body reaches the maximum.

(2) The vertical ice load is much greater than horizontal load, which should be considered as a principal factor in icebreaker design. Ice load mainly causes stress concentration at the stem post and outer shell around the bow.

(3) Ridge thickness directly determines the structural stiffness of ridge, which shows positive correlation with the ice load and energy absorption by the ridge. However, since the ship-ridge interaction area is mainly distributed around the ship hull, the effect of ridge thickness on ice load and energy absorption of ridge could be neglected when the ridge thickness exceeds 1.5 times the draft.

(4) The impact velocity represents the kinematic energy that ship initially carries. The number of impacts needed for the complete penetration of ridge is negatively correlated with impact velocity. High impact velocity will cause the local ice body around the hull to undergo large deformation and fragmentation in a short period of time, but it is difficult to cause obvious deformation of the entire ice body. Though higher impact velocity will cause higher ice load, the energy absorbed by the ridge is lower.

(5) Based on the analysis of ice load and energy absorption, it is suggested that ship should rush to the ridge with a lower velocity in the first collision and gradually speed up at the beginning of the subsequent collisions, so that the ice load is lower and the icebreaking efficiency could be improved.

References

[1] Heinonen J. Constitutive modeling of ice rubble in first-year ridge keel[R]. VTT Technical Research Centre of Finland, 2004.

[2] Gong H, Polojärvi A, Tuhkuri J. Discrete element simulation of the resistance of a ship in unconsolidated ridges[J]. Cold Regions Science and Technology, 2019, 167: 102855.

[3] Gong H, Polojärvi A, Tuhkuri J. Preliminary 3D DEM simulations on ridge keel resistance on ships[C]//International Conference on Port and Ocean Engineering Under Arctic Conditions, POAC, 2017.

[4] Zhou L, Gao J, Li D. An engineering method for simulating dynamic interaction of moored ship with first-year ice ridge[J]. Ocean Engineering, 2019, 171: 417-428.

[5] Timco G W, Burden R P. An analysis of the shapes of sea ice ridges[J]. Cold Regions Science and Technology, 1997, 25(1): 65-77.

[6] Leppäranta M, Hakala R. The structure and strength of first-year ice ridges in the Baltic Sea[J]. Cold Regions Science and Technology, 1992, 20(3): 295-311.

[7] Croasdale K R, Bruneau S, Christian D, et al. In-situ measurements of the strength of first-year ice ridge keels[C]//Proceedings of the International Conference on Port and Ocean Engineering Under Arctic Conditions, 2001.

[8] Shafrova S, Høyland K V. The freeze-bond strength in first-year ice ridges. Small-scale field and laboratory experiments[J]. Cold Regions Science & Technology, 2008, 54(1): 54-71.

[9] Yasunaga Y, Kioka S, Matsuo Y, et al. Tests on strength of consolidated parts of Hummock ice model[C]//Proceedings of the

International Conference on Port and Ocean Engineering Under Arctic Conditions, 2001.

[10] Serré N, Liferov P, Jochmann P. Model testing of ridge keel loads on structures Part III: Investigation of model ice rubble mechanical properties[C]//Proceedings of the International Conference on Port and Ocean Engineering Under Arctic Conditions, 2009.

[11] Kärnä T, Chae W R, Shkhinek K. Global loads due to first-year ice ridges[C]//The 16th International Conference on Port and Ocean Engineering Under Arctic Conditions (POAC), Ottawa, Canada, 2001: 627-638.

[12] Dolgopolov Y, Afanasiev V P, Koren′Kov V A, et al. Effect of hummocked ice on the piers of marine hydraulic structures [C]//3rd International Symposium on Ice Problems, Dartmouth College, Hanover, NH,1975.

[13] Croasdale K R, Cammaert A B. An improved method for the calculation of ice loads on sloping structures in first-year ice [J]. Hydrotechnical Construction, 1994, 28(3): 174-179.

[14] Soinen H, Nortala-Hoikkanen A. Development of ice model test into a reliable tool for icebreaking ship design[C]//ICETECH Symposium, Calgary, 1990.

[15] Brown T G, Croasdale K R, Wright B. Ice loads on the Northumberland strait bridge piers-An approach[C]//The Sixth International Offshore and Polar Engineering Conference, OnePetro, 1996.

[16] Ettema R, Huang H P. Ice-rubble accumulation beneath barges in ice-covered waters[J]. Journal of Hydraulic Research, 1988, 26(4): 397-412.

[17] Gurtner A, Evers K U, Repetto A. Ice rubble build-up on a shoulder ice barrier in shallow water[C]//19th IAHR International Symposium on Ice, (IAHR2008-006), 2008.

[18] Ince S T, Kumar A, Park D K, et al. An advanced technology for structural crashworthiness analysis of a ship colliding with an ice-ridge: Numerical modelling and experiments[J]. International Journal of Impact Engineering, 2017, 110: 112-122.

[19] Løset S, Kanestrøm Ø, Pytte T. Model tests of a submerged turret loading concept in level ice, broken ice and pressure ridges [J]. Cold Regions Science and Technology, 1998, 27(1): 57-73.

[20] Serré N, Liferov P, Evers K U. Model testing of ridge keel loads on structures Part I: Test set up and main results[C]//Proceedings of the International Conference on Port and Ocean Engineering Under Arctic Conditions(POAC09-78), 2009 .

[21] Bruun P K, Husvik J, Le Guennec S, et al. Ice model test of an Arctic SPAR[C]//Proceedings of the International Conference on Port and Ocean Engineering Under Arctic Conditions(POAC09-136), 2009 .

[22] Sawamura J, Tachibana T. Development of a numerical simulation for rotating and sliding of the ice floes along a ship hull [C]//Proceedings of the International Conference on Port and Ocean Engineering Under Arctic Conditions(POAC11-036), 2011 .

[23] Molyneux D, Spencer D, Liu L. Loads due to first year ice ridges on a vertical cylinder[C]//International Conference on Offshore Mechanics and Arctic Engineering, American Society of Mechanical Engineers, 2013.

[24] Polojärvi A. Sea ice ridge keel punch through experiments: Model experiments and numerical modeling with discrete and combined finite-discrete element methods[D]. Aalto University, 2013.

[25] Serré N. Mechanical properties of model ice ridge keels[J]. Cold Regions Science and Technology, 2011, 67(3): 89-106.

[26] Zhao W, Johan Leira B, Vilhelm Høyland K, et al. On the structural analysis of icebreakers due to ramming of first-year ice ridges[C]//International Conference on Offshore Mechanics and Arctic Engineering, American Society of Mechanical Engineers, 2022.

[27] Timco G W, Croasdale K, Wright B. An overview of firstyear sea ice ridges[J]. PERD/CHC Report, 2000, 5:112- 159.

[28] Ettema R, Urroz G E. On internal friction and cohesion in unconsolidated ice rubble[J]. Cold Regions Science and Technology, 1989, 16(3): 237-247.

[29] Timco G W, Cornett A M. Is φ a constant for broken ice rubble[C]//Proceedings of the 10th Workshop on River Ice Management with a Changing Climate Winnipeg, Manitoba, Canada, 1999.

[30] Wong T T, Morgenstern N R, Sego D C. A constitutive model for broken ice[J]. Cold Regions Science and Technology, 1990, 17(3): 241-252.

[31] ISO 19906. Petroleum and natural gas industries-Arctic offshore structures[S]. International Organization for Standardization, 2010.

[32] Lewis R W, Schrefler B A. The finite element method in the static and dynamic deformation and consolidation of porous me-

dia[M]. John Wiley and Sons, 1998.

[33] Hellman J H. Basic investigations of mush ice[C]//Proceedings of the IAHR International Symposium on Ice, Hamburg, Germany, 1984.

[34] Kulyakhtin S, Høyland K V. Ice rubble frictional resistance by critical state theories[J]. Cold Regions Science and Technology, 2015, 119: 145-150.

[35] Liu Z. Analytical and numerical analysis of iceberg collisions with ship structures[D]. Norwegian University of Science and Technology, 2011.

[36] Gao Y, Hu Z, Ringsberg J W, et al. An elastic-plastic ice material model for ship-iceberg collision simulations[J]. Ocean Engineering, 2015, 102: 27-39.

[37] Motora S. On the measurement of added mass and added moment of inertia of ships in steering motion[C]//Proceedings of the First Symposium on Ship Maneuverability, David Taylor Model Basin, 1960.

[38] Gao Y. An elastic-plastic ice material model and iceberg shape sensitivity analysis for ship-iceberg collision scenario[D]. Shanghai: Shanghai Jiao Tong University, 2015.

极地船舶与冰脊多次碰撞的数值模拟

贾 宾[1], 鞠 磊[1], 石 莉[2], 王 庆[1], 庞福振[1]

(1. 哈尔滨工程大学 船舶工程学院, 哈尔滨 150001; 2. 美国船级社(中国)有限公司, 上海 200001)

摘要: 极地船舶在冰区航行时将不可避免地与冰脊发生相互作用。相比于其他类型的冰体,冰脊由于其尺度与结构特点,呈现出更为复杂的力学特性。本文采用非线性有限元方法研究极地船舶与冰脊之间的相互作用。基于弹塑性模型建立冰脊模型,并选取Drucker-Prager屈服准则,同时考虑粘聚力、摩擦角以及硬化的影响。将开发的材料模型嵌入LS-DYNA中,通过半隐式图形返回算法进行求解。通过模拟冰脊与船舶的多次碰撞,评估冰脊和船体的应力分布以及冰载荷的时历变化。此外,通过参数化分析,讨论冰脊厚度和冲击速度对冰载荷和吸能结果的影响。

关键词: 冰脊; 船舶; 非线性有限元; 冰载荷; 相互作用; 强度

中图分类号: P731.15 P751 **文献标识码:** A

基金项目: 国家自然科学基金资助项目(52192690;52192695)

作者简介: 贾 宾(1994-),男,博士研究生;

鞠 磊(1986-),男,博士,哈尔滨工程大学副教授。